This is a repository copy of *Optimum resistive loads for vibration-based electromagnetic energy harvesters with a stiffening nonlinearity*.

White Rose Research Online URL for this paper:
http://eprints.whiterose.ac.uk/81370/

Version: Accepted Version

Article:

Optimum resistive loads for vibration-based electromagnetic energy harvesters with a stiffening nonlinearity

A. Cammarano,* S. A. Neild,
S. G. Burrow, D. J. Wagg, and D. J. Inman

Abstract

The exploitation of nonlinear behavior in vibration-based energy harvesters has received much attention over the last decade. One key motivation is that the presence of nonlinearities can potentially increase the bandwidth over which the excitation is amplified and therefore the efficiency of the device. In the literature, references to resonating energy harvesters featuring nonlinear oscillators are common. In the majority of the reported studies, the harvester powers purely resistive loads. Given the complex behavior of nonlinear energy harvesters, it is difficult to identify the optimum load for this kind of device. In this paper the aim is to find the optimal load for a nonlinear energy harvester in the case of purely resistive loads. This work considers the analysis of a nonlinear energy harvester with hardening compliance and electromagnetic transduction under the assumption of negligible inductance. It also introduces a methodology based on numerical continuation which can be used to find the optimum load for a fixed sinusoidal excitation.

Keywords: energy harvesting, nonlinear dynamics, optimization, continuation, electrical load.

1 Introduction

As the power consumption of wireless electronic devices reduces, the potential of powering them from energy harvested from the environment, rather than from batteries, increases. One often-cited source of ambient energy is structural vibration: power-autonomous systems, such as distributed sensor networks, powered by structural vibrations have been reported in many recent works in the literature (for example Torah et al. 2008 and Roundy and Wright 2004).

The ability to harvest vibration energy depends heavily upon the form of the vibrations. Furthermore the harvester needs to be compatible with at least one of the established techniques to electrically damp the oscillation. For example, the majority of published works present vibration harvesters based upon mechanical oscillators (boosting the amplitude of vibration and enabling efficient electrical transduction). However this arrangement implies that only vibrational

---

*Corresponding author. email: `andrea.cammarano@bristol.ac.uk`

1

energy close to the resonant frequency of the oscillator can be harvested efficiently. Since the resonance bandwidth is generally narrow to achieve the amplification required, the harvester must be carefully tuned to the required vibration frequency (Williams and Yates 1996, Baker et al. 2005, Stephen 2006, Renno et al. 2009).

One topic which several researchers have explored to widen the application of vibration harvesters is the use of nonlinear oscillators (Burrow and Clare 2007, Mann and Sims 2009, Stanton et al. 2010, Cottone et al. 2009, Erturk et al. 2009, Daqaq et al. 2009). Nonlinear oscillators are known to exhibit broad bandwidths under certain conditions and hence it may be possible to exploit this feature to maximize the harvestable energy where the source vibrations vary in frequency. Compared to linear-oscillator based energy harvesters, nonlinear devices display more complex behaviors and thus the modeling and simulation is more involved, making it difficult to define and then find the set of optimal parameters (mechanical and electrical) for energy generation.

In addition to enabling the purposeful design of harvesters with nonlinearity, understanding their behavior is important since some harvesters will feature nonlinear behavior as a result of manufacturing, or as a consequence of another design choices. For example the device described and modeled by the authors in Cammarano et al. 2011 uses high permeability magnetic materials in the transducer to improve electromagnetic coupling but results in the device exhibiting highly nonlinear compliance characteristics.

Much of the work in the literature considers the dynamic response of nonlinear energy harvesters with simplified electrical loads (Triplett and Quinn 2009, Barton and Burrow 2010, Karami and Inman 2011, Liao and Sodano 2009). In this paper the definition and determination of a purely resistive load that results in the maximum harvested power is considered. The method introduced is general and can be applied to either one parameter or multiple parameters: an example of a two-parameter optimization is shown later. In Section 2, a short description of the load optimization for linear energy harvesting is provided. In Section 3 the main differences between the linear and the nonlinear case are presented and methods for investigating the optimum parameters are introduced. These allow the selection of the linear natural frequency and resistive load that result in a nonlinear harvester operating at maximum power. Moreover, this work provides useful information for developing control strategies for improving the efficiency of existing devices that exhibit nonlinear behavior. The results obtained with the two-parameter optimization are compared with the power harvested by an optimized linear harvester in Section 4 and conclusions are drawn in Section 5.

2 Linear harvester: optimum resistance

Harvesting energy from vibrations relies on the fact that the energy of the primary structure can be transferred to a transducer, and thereby converted into electric energy. For this purpose an oscillator tuned to the frequency of excitation can be used. In other words a linear energy harvester can be thought of as a base-excited oscillator coupled with a transducer. The coupling between the oscillator and the transducer can be represented by the force F_e with which the transducer responds to the relative movement of the oscillating mass (see
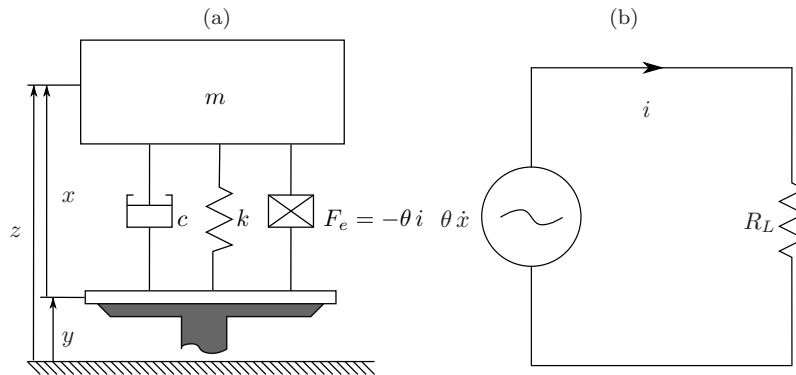
FIGURE 1: Schematic of a linear energy harvester powering a purely resistive load.

Figure 1). This leads to the mechanical dynamics

$$m\ddot{x} + c\dot{x} + kx = -m\ddot{y} + F_e, \tag{1}$$

where m is the mass of the oscillator, c is the mechanical damping, k the stiffness of the spring. The variable x measures the relative distance between the harvester mass and the moving base and y is the displacement of the base with respect to the inertial reference frame. In the case of an electromagnetic transducer, the coupling force is due to electromagnetic interaction between the magnet and the current i induced in the coil and can be written as follows

$$F_e = -\theta i, \tag{2}$$

where θ is the electromechanical constant.

Two common designs for the electromagnetic transducers are found in the literature. In the first configuration the magnet is fixed to the frame of the harvester and the coil moves with the oscillating mass. In the second one the coil is fixed to the frame and the magnet moves with oscillating mass. In both cases, the mass of the moving part of the transducer has to be taken into account for the correct design of the moving mass. In either configuration, the motion of the oscillating mass induces a change in the relative position between the magnet and the coil, and by Faraday's law, a voltage proportional to the change of the flux linked with the coil is induced. If the terminals of the coil are not connected to any circuit, ideally no current can pass through the coil and the tension is proportional to the velocity of the coil: $v = \theta\dot{x}$. When the coil is connected to a purely resistive load, the value of i can be evaluated by using Kirchhoff's second law,

$$\theta\dot{x} = R_L i. \tag{3}$$

We note that more complex loads and optimized circuits for power conditioning have been presented in the literature (Wickenheiser and Garcia 2010). The choice of simplifying the load to a pure resistance is aimed at providing a valid comparison between the nonlinear harvester and the well reported case of a linear harvester with resistive load. This simple load case provides insight into

3

the additional complexity of designing harvesters with nonlinear elements. For the same reason an ideal coil, which has no parasitic resistance, is considered. [assumed]

The electric force due to the reactive component is very small over the frequency range of interest given the resistance values considered (0.03% of the elastic force). For this reason the inductance of the coil is neglected as well. Note that for harvesters with extremely low levels of mechanical damping and parasitic resistance or operating at high frequency the reactive force is not negligible. These cases are not considered in this work. Using Equation (2) and (3), it is possible to relate the electromagnetic force to the velocity of the harvester. The expression obtained, substituted in Equation (1) leads to

$$m\ddot{x} + \left(c + \frac{\theta^2}{R_L}\right)\dot{x} + kx = -m\ddot{y}. \tag{4}$$

By inspection of Equation (4), it can be seen that the electromagnetic interaction, in this case, is perceived as a damping force acting on the harvester mass. Figure 2a shows a schematic of the equivalent mechanical oscillator with two dampers in series. Using the mobility analogy on this system it can be shown
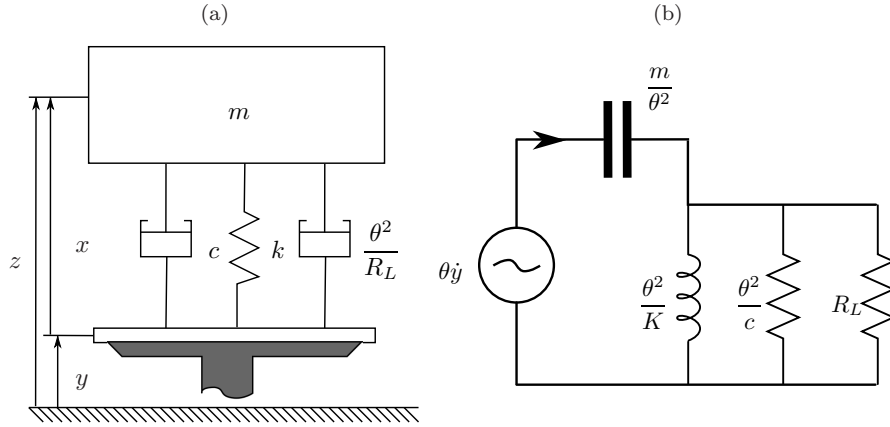

FIGURE 2: Mechanical (a) and electrical (b) analogy of the energy harvester with a purely resistive load

that the circuit in Figure 2b is the electrical equivalent to Figure 2a. In the analogy, the current circulating in the circuit is proportional to the force applied to the system and the voltage generated is proportional to the velocity. Applying Thevenin's theorem to the circuit it can be proved that the maximum energy dissipated in the load is obtained when the value of R_L is equal to θ^2/c. This same result can be obtained analytically by applying the Fourier transform to Equation (4), resulting in

$$\left(-m\Omega^2 + \left(c + \frac{\theta^2}{R_L}\right)j\Omega + k\right)X(\Omega) = m\Omega^2 Y(\Omega). \tag{5}$$

Finding the value of $X(\Omega)$ from Equation (5) and substituting it into Equation (3) allows the Fourier transform of the current to be obtained. Hence, the

average power dissipated in the electrical load over a cycle can be evaluated as

$$P = \frac{1}{2} R_L I^2 = \frac{\left(\theta m \Omega^3 |Y(\Omega)|\right)^2}{2 R_L \left[(k - m\Omega^2)^2 + \left(c + \dfrac{\theta^2}{R_L}\right)^2 \Omega^2\right]}. \tag{6}$$

Considering a constant amplitude of base displacement, the value of R_L which allows for the power in the load to reach its maximum can be found using Fermat's theorem on the stationary points for n-dimensional functions

$$\left\{\frac{\partial P}{\partial R_L}, \frac{\partial P}{\partial \Omega}\right\} = \mathbf{0} \quad \Leftrightarrow \quad \left\{R_L = \frac{\theta^2}{c}, \Omega \approx \sqrt{\frac{k}{m}}\right\}. \tag{7}$$

This means that the energy harvester gives the maximum power to the load if operated at its natural frequency and that the losses in the electrical resistance and in the mechanical damping have to be equal.[1]. As previously mentioned this work considers an harvester with an ideal coil. The coil resistance can be taken into account by scaling the power multiplying by the ratio between the effective load resistance and the total resistance. This is thoroughly demonstrated in Stephen 2006. A more exhaustive discussion about the optimum load for linear energy harvesters can be found in Cammarano et al. 2010.

3 Nonlinear harvester: load optimization

In this section a mathematical model of a nonlinear energy harvester with cubic stiffness is presented. An example of this type of harvester along with experimental validation is given by Burrow and Clare 2007. The model is based on the following second order differential equation

$$m\ddot{x} + \left(c + \frac{\theta^2}{R_L}\right)\dot{x} + kx + k_{nl}\, x^3 = -m\ddot{y}. \tag{8}$$

where m is the moving mass and c the mechanical damping coefficient. The equivalent elastic force $k\,x + k_{nl}x^3$ is the composition of the mechanical stiffness of the system and the component of the magnetic force in phase with the displacement. For more details on this topic see, for example, Cammarano et al. 2011. Equation (8) can be written in terms of non-dimensional parameters as follows

$$\ddot{x} + 2\,\omega_n\,\zeta_t\,\dot{x} + \omega_n^2\,x + \alpha\,x^3 = -\ddot{y}, \tag{9}$$

where ω_n is the linear natural frequency of the system, $\alpha = k_{nl}/m$ and ζ_t is the damping ratio. The damping ratio represents both the electrical and the mechanical losses, hence

$$\zeta_t = \frac{1}{2\,m\,\omega_n}\left(c + \frac{\theta^2}{R_L}\right). \tag{10}$$

---

[1]The optimal frequency is not exactly equal to the natural frequency, it is slightly higher due to damping. Nevertheless, since the oscillator is designed so that it can amplify the input excitation, the total damping has to be small and therefore the use of the undamped natural frequency can be justified

3.1 Analytical model

The nonlinear differential Equation (9) can be solved using the analytical approximate method of nonlinear normal forms (NLNF), described in Neild and Wagg 2011.

For the NLNF method to be valid the contribution of the nonlinear terms has to be small when compared to the other terms. This assumption is not always true for this application: when the system is considered open-circuit (i.e. the mechanical damping is the only loss mechanism in the system), the nonlinear elastic force can be of the same order of magnitude as the linear elastic force. However this does not affect the computation of the primary response (see Neild and Wagg 2013). To confirm this, an error analysis is presented in Section 3.5. Also, when a load resistance is considered in the circuit, the total damping of the device increases such that the amplitude of the oscillations, as well as the ratio between nonlinear and linear forces, reduces. In Neild and Wagg 2011 the method is described for a sinusoidal force. Here the system is base-excited. For the case where base moves sinusoidally, the forcing term can be written as follows

$$F = -\Omega^2 Y_o \cos\left(\Omega t\right), \tag{11}$$

where Y_o is the maximum displacement of the base with respect to the inertial reference frame. Hence, equation (9) can be written as

$$\ddot{x} + 2\,\omega_n\,\zeta_t\,\dot{x} + \omega_n^2\,x + \alpha\,x^3 = -\Omega^2 Y_o \cos\left(\Omega t\right). \tag{12}$$

Here the damping ratio ζ_t and the nonlinear coefficient α in this model are assumed to be small compared to the other terms. Following the procedure in Neild and Wagg 2011, or using the general solution for polynomial nonlinearities reported in Xin et al. 2013, the amplitude of the oscillation can be related to the input excitation by

$$\left(\left(\omega_n^2 - \Omega^2\right) U + \frac{3}{4}\,\alpha\,U^3\right)^2 + \left(2\,\zeta_t\,\omega_n\,\Omega\,U\right)^2 = \left(-\Omega^2 Y_o\right)^2, \tag{13}$$

where U is the amplitude of the first harmonic. The components of the response at harmonics of the forcing frequency can also be calculated (Neild and Wagg 2011). For sake of simplicity, in this paper, to estimate the harvested power equation 13 is used, and the higher order harmonics are neglected.

3.2 Optimum resistance

Although the oscillator is nonlinear, Equation (3) still holds. Assuming that the amplitude of x equals U, i.e. neglecting the contribution of the higher harmonics, Equation (3) can be written as

$$P = \frac{1}{2}\,\frac{\left(\Omega\,U\right)^2\,\theta^2}{R_L}. \tag{14}$$

From Equation (14) an expression for U^2 as a function of P can be derived, which, substituted into Equation (13), leads to

$$2\left(\left(\omega_n^2 - \Omega^2\right) + \frac{3}{2}\,\frac{\alpha\,R_L P}{\theta^2\Omega^2}\right)^2 \frac{R_L P}{\theta^2\Omega^2} + 2\left(\frac{c}{m} + \frac{\theta^2}{R_L m}\right)^2 \frac{R_L P}{\theta^2} = F^2. \tag{15}$$

Equation (15) provides a functional relationship between the power P and the load resistance R_L. To find this relationship, it is necessary to find the roots of a cubic equation, which leads to overly lengthy expressions providing limited insight about the dependency between the power delivered to the load and its resistive characteristics. In addition the differentiation of these expressions with respect to R_L results in 6th order polynomials. The roots of these would require numerical evaluation. This would reduce the advantage of using an analytical method. A different approach is therefore adopted. Rearranging Equation (15) to be in the form

$$G(P, R_L) = 0 \tag{16}$$

the implicit function theorem can be applied. The derivative of the power with respect to the load resistance can be evaluated using

$$\frac{\partial P}{\partial R_L} = -\frac{\dfrac{\partial G}{\partial R_L}}{\dfrac{\partial G}{\partial P}}. \tag{17}$$

The stationary points of the function $P(R_L)$ coincide with the zeros of Equation (17). To express the results of this analysis in a more compact way, the following coefficients have been defined

$$a_1 = \frac{9}{2}\left(\frac{\alpha}{\theta^3 \, \Omega^3}\right)^2,$$

$$a_2 = \frac{6\,\alpha}{\theta^4}\,\frac{\omega_n^2 - \Omega^2}{\Omega^4},$$

$$a_3 = \frac{2}{\theta^2}\left[\left(\frac{\omega_n^2 - \Omega^2}{\Omega}\right)^2 + \left(\frac{c}{m}\right)^2\right],$$

$$a_4 = \frac{4\,c}{m^2},$$

$$a_5 = \frac{2\,\theta^2}{m^2}.$$

so that Equation (15) can be written as

$$G(P, R_L) = a_1 R_L^3 P^3 + 2 a_2 R_L^2 P^2 + \left(a_3 R_L + a_4 + \frac{a_5}{R_L}\right) P - F^2. \tag{18}$$

Hence the numerator of Equation (17) can be written as

$$P(3\,a_1\,R_L^4\,P^2 + 2\,a_2\,R_L^3\,P \, + \, a_3\,R_L^2 \, - \, a_5\,)R_L = 0. \tag{19}$$

Equation (19) provides a relation between P and R_L which applies when the function $P(R_L)$ is at a maximum, given by

$$P = \frac{1}{3}\,\frac{-a_2 R_L + \sqrt{(a_2^2 - 3a_1 a_3)R_L^2 + 3a_1 a_5}}{a_1 R_L^2}. \tag{20}$$

By substituting Equation (20) into Equation (18), a 6th order polynomial in R_L is obtained. Not all the solutions of this polynomial are values of optimal

Linear stiffness	300	N/m
Nonlinear stiffness	1.02×10^8	N/m^3
Mechanical damping	4.8	Ns/m
Electro-mechanical coefficient	8.9	Vs/m

TABLE 1: Mechanical and electrical parameters used for the model of the nonlinear harvester

resistances. Roots which are negative or complex must be discarded as non-physical and in addition those relative to the minima are of no interest.

To proceed we consider an example system in which the equivalent force-displacement curve has a cubic characteristic. The parameters for the mathematical model, taken from an experimental characterization of a real device (Cammarano 2012), are listed in Table 1. The device considered has an underlying linear frequency of ~ 10 Hz. All the parameters in Equation (18) are fixed except for the frequency of excitation, which is varied between 5 and 25 Hz. For each frequency, the roots of the polynomial have been extracted using the function "roots" provided by MATLAB based on the extraction of the eigenvalues of the companion matrix associated with the polynomial. Keeping just the valid (real, positive) roots, these are substituted, using an iterative routine, into Equation (20) and the corresponding values of power found. Figure 3 shows the resulting power harvested as a function of frequency for a range of resistive loads (grey and red lines representing stable and unstable solutions respectively). Unlike the linear case, the maximum power is not obtained at the same frequency, a projection of the maximum power from the 3D plot is shown as a thick black line on the power-frequency plane. This relationship requires the optimum resistance to be used. The relationship between the optimum resistance, the frequency and power is shown as thick black lines in the frequency-resistance and power-resistance plane respectively.

Figure 4a, again shows the power harvested as a function of frequency for a range of resistive loads, but now we consider the case where the frequency is fixed. Two such slices are shown as thick black lines on the plot. The curves relating to $f = 11.7$ Hz and $f = 18$ Hz are shown in detail in Figure 4b and 4c respectively. It can be seen that for low resistance values the system is heavily damped: here only one positive real root for the resistance is found and it corresponds to a maximum. This is the case in which the amplitude of the oscillations is small and the system behaves like a linear harvester.

As the resistance increases, the amplitude of oscillation also increases and the contribution of the nonlinear terms to the behavior of the harvester becomes more influential. After the fold in the frequency response, more than one stable solution appears for the oscillation and hence, also for the power. Of all the possible solutions, only one corresponds to the absolute maximum, all the other solutions (grey lines in the figures) are neglected.

This can be seen in more detail in Figure 4b and 4c, where the power versus resistance at fixed frequency of excitation is shown. This corresponds to a cut of the surface in Figure 4a with a plane perpendicular to the frequency axis. For those frequencies where unstable branches exist, the cut reveals that the
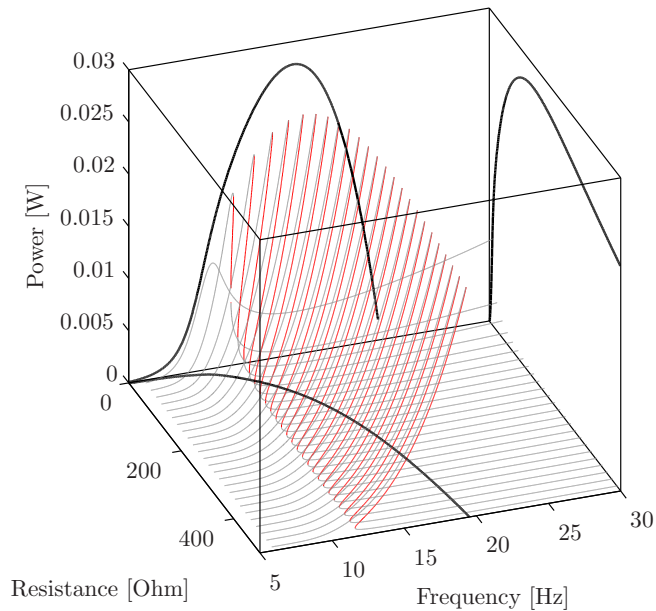
FIGURE 3: Power surface: the thin lines show the average harvested power per cycle over a range of resistance values (the gray and red lines represents stable and unstable solutions respectively). For each of these curves, the point at which the harvested power is at a maximum for a given resistance is identified. The locus of these points is shown as a projection onto the frequency-power, frequency-resistance and resistance-power plane (thick black lines).

curves have both a maximum and a minimum (see Figure 4b). Interestingly the resistance corresponding to the minimum quickly becomes very high as the frequency is increased: in Figure 4c the minimum is beyond the resistance range considered here.

Figure 4 also shows the reason why the optimal power and the optimal resistance change with the frequency of excitation. In fact, unlike the linear case, the power surface is skewed because of the influence of the resistance on the peak position. This is clarified in more detail in the following section.

3.3 Physical interpretation

The relationship between resistive load and the response of a nonlinear harvester is complicated. Unlike in a linear system, the resistance affects not only the amplitude of the response but also the shape of the entire frequency response. In the case of a harvester with a fixed hardening stiffness, for example, the damping determines how much the resonant peak is "bent" and therefore the existence of folding points and unstable branches. As previously discussed, the optimal load depends on the frequency of excitation and it is therefore interesting to consider. This leads to the question of what happens if the load is optimized at input frequency Ω_1 and the system is excited at a different frequency.

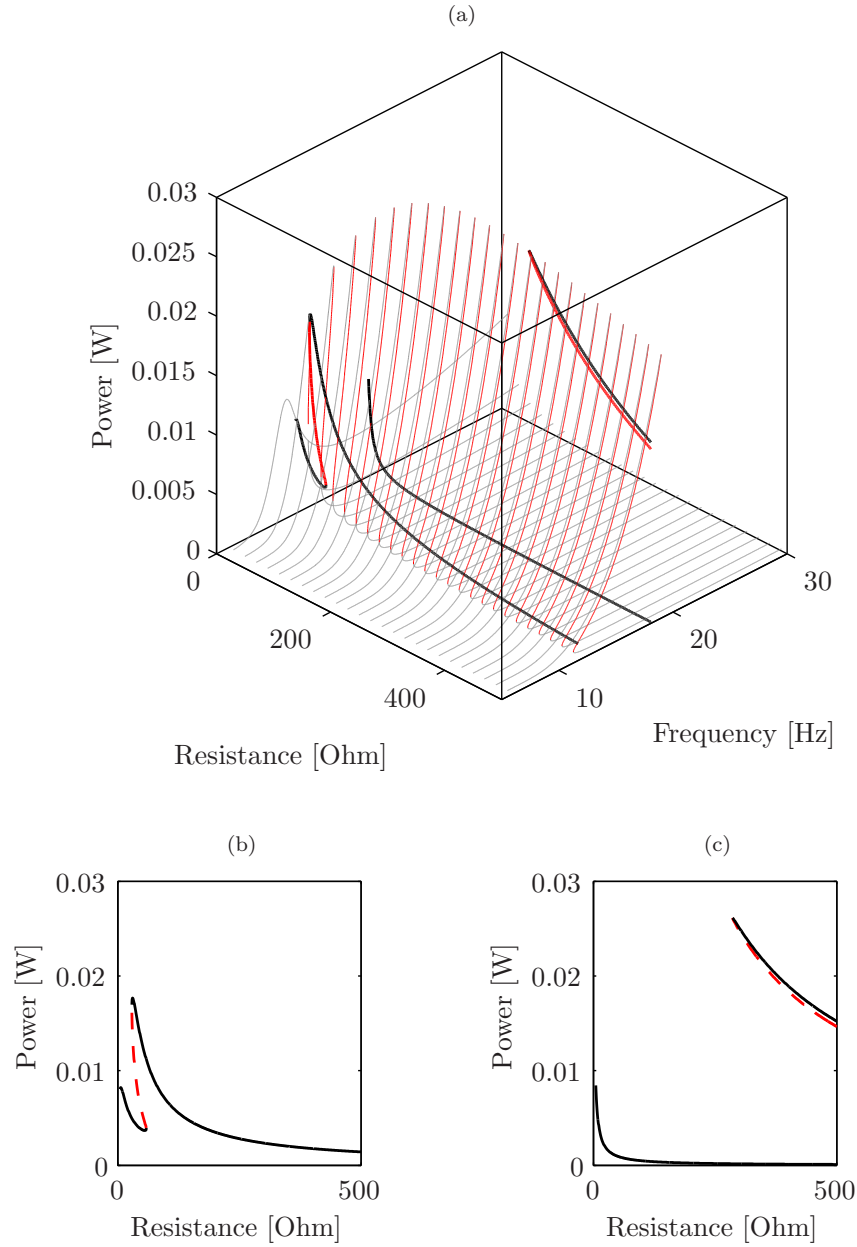Figure (5) shows that when the load is optimized for a given frequency

FIGURE 4: Power surface (a): the thin lines show the average harvested power for a cycle over a range of resistance values. The thick black lines are the intersections of the surface with two vertical planes at frequency $f = 11.7$ Hz and $f = 18$ Hz. Panels (b) and (c) shows the curves in greater detail. Here the dashed red lines are representative of the planes cutting through the unstable region.

$\Omega_1 > \omega_n$ the resonant peak of the frequency response reaches its maximum at Ω_1. In other words, optimal resistance is such that the maximum amplitude of oscillation occurs at the optimized frequency. This behavior indicates another
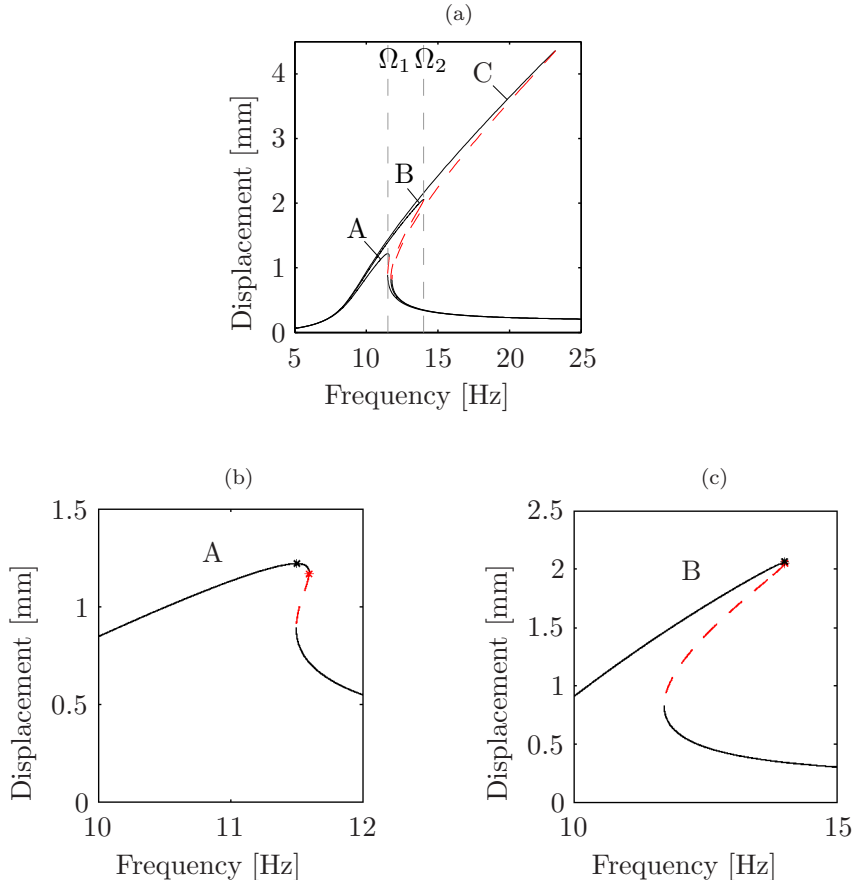

FIGURE 5: Effect of the optimum resistance on the frequency response. When the resistance is optimized for a given input frequency Ω, the peak of the frequency response moves along the backbone of the system so that the frequency at which maximum displacement occurs corresponds to the chosen input frequency. (a) shows the frequency response of the system where the optimization has been performed at (A) $\Omega_1 = 11.5Hz$ ($R_{opt} = 26.75$ Ohm) and (B) $\Omega_2 = 14.5Hz$ ($R_{opt} = 75$ Ohm) . The response of the system open circuit is labeled with (C). (b) shows details of the curve (A) and (c) shows curve (B). The dashed red curves represents the unstable branches whereas the stable solutions are shown with black solid lines. The red and the black stars show the position of the folding point and the maximum power respectively.

possible advantage of nonlinear harvesters: the degree of frequency tuning can be achieved by modifying the load resistance, and without the need to employ reactive loads as required for linear harvesters. The frequency range in which the harvester can be tuned, in the case of a hardening stiffness, spans between

ω_n and the frequency at which the folding point at $R_L = \infty$ occurs (i.e. the range is limited by the mechanical damping of the system).

A drawback of this result is that the power output reaches its maximum in the proximity of the folding point: in this region a low amplitude stable oscillation exists and even a small perturbation can force the system toward this undesirable response. A feedback control can be used to ensure that the system remains on the high power branch, but the design of such a controller is beyond the scope of this work.

The vicinity of the maximum achievable power to the folding point is a feature which can be used to simplify the numerical evaluation. This is discussed in the next section and allows for rapid identification of the optimal load and power for a given excitation frequency. Then in Section 3.5 a purely numerical method is presented and used to assess the accuracy of the approximate approach.

3.4   Simplified formula

In this section a simplified formula for the optimal resistance is presented. The formula relies on the approximation that the maximum power is obtained when the system is at resonance and therefore the external force is in phase with the damping force. Using Equation (13) and splitting the conservative terms

$$\left(\omega_n{}^2 - \Omega^2\right) U + \frac{3}{4}\alpha U^3 = 0 \tag{21}$$

from the non-conservative forces and balancing the non-conservative force with the external force the following equation is obtained

$$2\,\zeta_t\,\omega_n\,\Omega\,U = -\Omega^2 Y_o. \tag{22}$$

From Equation (21) a relation between the amplitude of oscillation U and the frequency Ω is found

$$U = \sqrt{\frac{4}{3\alpha}\left(\omega_n{}^2 - \Omega^2\right)}. \tag{23}$$

This curve is termed the backbone curve and it gives information of the oscillations the system would exhibit if it were unforced and undamped. By substituting Equation (23) into Equation (22) and recalling that the total damping is the sum of the mechanical and the electrical damping (Equation (10)), an expression for the optimal R_L can be found

$$R_L = \frac{\theta^2}{m}\left(\frac{2\left(\Omega^2 - \omega_n^2\right)}{\Omega\,Y_0\sqrt{3\,\alpha\,\left(\Omega^2 - \omega_n^2\right)} - 2\,\zeta_m\,\omega_n\,\left(\Omega^2 - \omega_n^2\right)}\right). \tag{24}$$

Equation (24) relates the optimal resistance to the other parameters of the system. The accuracy is assessed in Figure 6 which shows a comparison of the results previously shown in Figure 3 (thick black lines) with the curves obtained from the simplified formulation (red dashed lines).

The formula gives accurate results over a frequency range spanning resonance, i.e. over the region of primary interest. The reason for this is that the simplified formula is based on the assumption that the maximum electrical power is obtained when the excitation frequency is very close to the jump-down
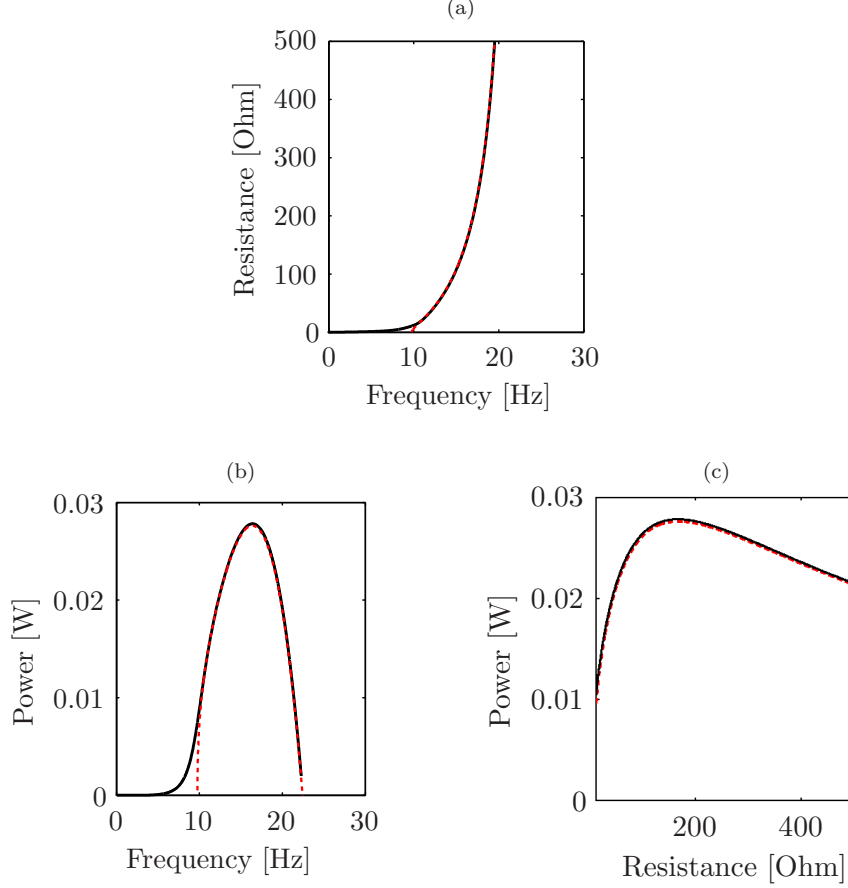
FIGURE 6: Simplified formula given in Equation 24: the projection of the locus of maximum power is projected in the frequency vs resistance plane (a), frequency vs power (b) and resistance vs power (c). The solid black line represents the solution of the NLNF whereas the dashed red line represents the solution found with the simplified formula.

frequency. Since all the other parameters are fixed, only one value of total damping allows this to happen. The optimal resistance is therefore the resistance that together with the mechanical damping, achieves the required total damping and it is given by

$$R_L = \frac{\theta^2}{c_T - c_m}. \tag{25}$$

From Equation (24), rearranging the terms and simplifying leads to

$$R_L = \frac{\theta^2}{\dfrac{m\,Y_0\,\Omega\,\sqrt{3\,\alpha}}{2\,\sqrt{\Omega^2 - \omega_n^2}} - c_m}. \tag{26}$$

13

By comparing Equation (25) and (26), it can be seen that

$$c_T = \frac{m\,Y_0\,\Omega\,\sqrt{3\,\alpha}}{2\,\sqrt{\Omega^2 - \omega_n^2}}.$$

(27)

Note that if the system is linear ($\alpha = 0$), this formula cannot be used: both the numerator and the denominator of the expression for c_T become zero. For this case there is no jumping-down frequency and therefore the hypotheses behind the simplification are not satisfied.

From the formula, it is clear that when $\Omega < \omega_n$, no solution exists for the case where $\alpha > 0$ (i.e. the stiffness is hardening). This sets the lower limit of the frequency range in which the formula can be used. The upper limit is determined by the fact that the value of the resistance has to be positive, hence $c_T > c_m$. This gives the validity region

$$\Omega < \omega_n \left(1 - \frac{3}{4}\frac{Y_0^2\,m^2\,\alpha}{c_m^2}\right)^{-\frac{1}{2}}.$$

(28)

The frequency domain of the formula can be seen clearly in Figure 6b, where the formula provides results between approximately 10 Hz and 23 Hz.

3.5   Continuation method

The method used in this analysis is developed using the assumption of weak nonlinearity. In order to verify the accuracy of the results, the theoretical relations are compared with numerical results. The system has been analyzed with Auto07p, a software package based on numerical continuation of ordinary differential equation, Doedel et al. 1997. Auto07p is capable of continuing periodic orbits. The initial orbit for the continuation is computed by integrating Equation 12 with the *ode45* routine provided by MATLAB. For the initial simulation the frequency of excitation was set to 5 Hz and the load resistance to 1MOhm. Such a high value of resistance is used to approximate open-circuit conditions.

First, continuation of the initial orbit is performed considering the resistance R_L as the varying parameter. Then, the solutions of the first continuation are used as the initial solution for generating the relationship between power (average over a period) and frequency response, see Figure 7b. For each curve, the resistance is kept constant and the frequency is changed.

As noted in Section 3.3, the maximum power is delivered to the load almost at the frequency where the fold in the frequency response occurs. Hence, the envelope of the maximum power (black solid line in Figure 7) has been computed via continuation of the orbit corresponding to the folding point for different values of load resistance. This approximation is valid when the total damping of the system is small, i.e. the load resistance is high. Note that it is not capable of predicting the maximum power when no fold in the frequency response exists (for this case, when the load resistance is lower than 10 Ohm). For $R_L > 10$ Ohm the continuation method predicts two solutions: one for the upper fold, corresponding to the high power solution and therefore of interest, and one for the lower fold.

The maximum power has also been computed using time simulations stepping over the resonant frequency response. Using this as the benchmark, the
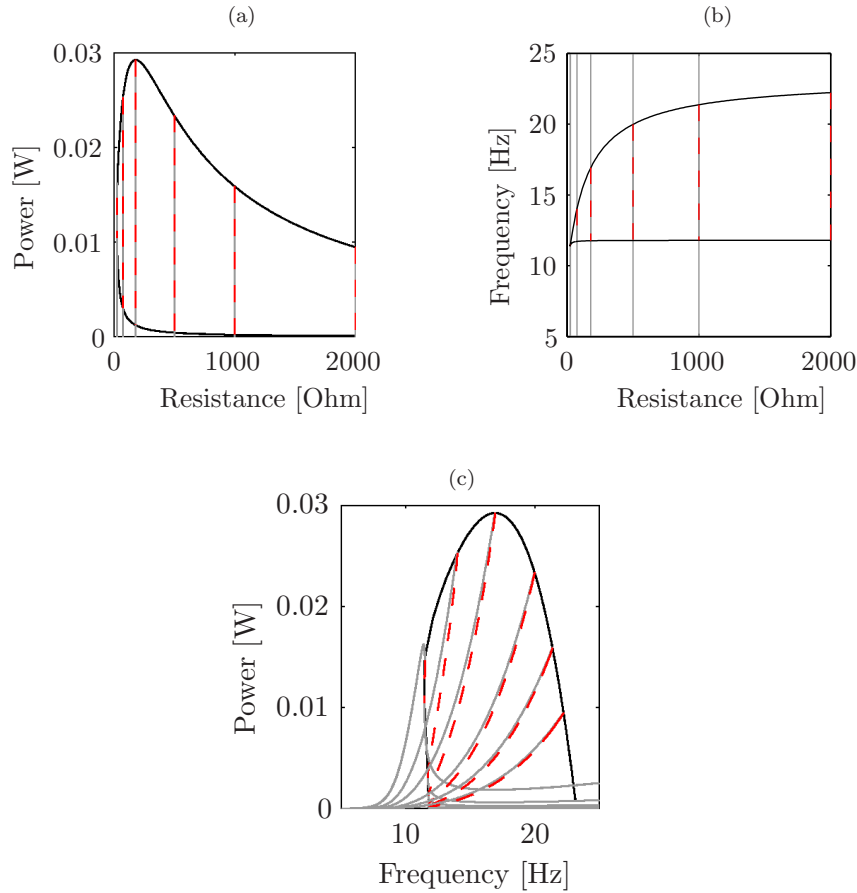
14

FIGURE 7: Numerical continuation: (a) power reached at the folding point for different values of resistance and (c) projection on the frequency-power plane. In each figure both the stable (solid grey) and the unstable (dashed red) solutions are shown. (b) shows the extent of the frequency region in which unstable solutions exist.

maximum error due to approximating the maximum power to that at the fold is less than 0.07% in a range of ±30 Ohm about the optimal resistance. In the same resistance range, the difference between the solutions obtained using Auto07p and the NLNF is 0.69 % (if the third harmonics are included in the NLNF solution, 3% if these are neglected).

Figure 8 shows the comparison between the upper fold solution obtained with Auto07p and the maximum power predicted using Equation (24). In this case the difference between the two solutions never exceeds 5 %. This shows that the simplified formula can be used for choosing the optimal load for the device. In fact, as shown in Figure 8b, although the simplified model underestimates the optimum resistance value, the power-resistance curve has a small derivative around its maximum which means that the power lost by selecting the underestimate of the resistance is relatively small.
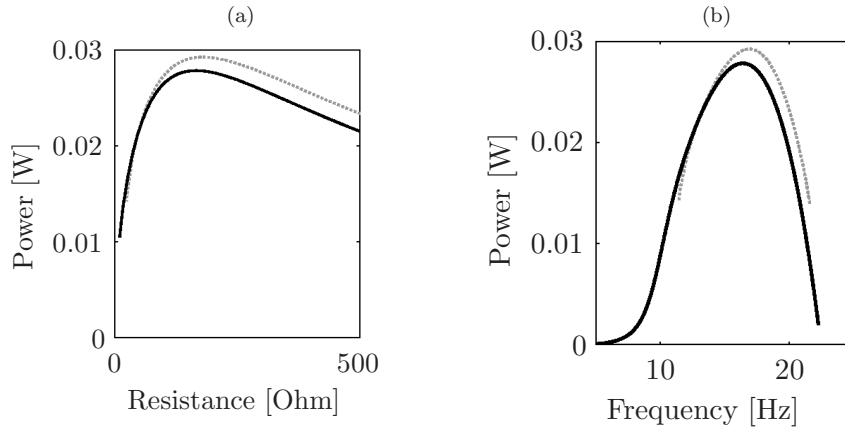
15

FIGURE 8: Comparison between the analytical and the numerical results: power achieved with the optimal resistance (a) and projection on the frequency-power plane (b). In both figures the numerical continuation results are represented with dashed grey lines whereas the black solid line shows the analytical results using the simplified formula.

4   Two parameter-optimization

So far in this paper, the effects of the resistance on the power output of a nonlinear energy harvester have been investigated. In this section the effect of changing both the resistance and the linear stiffness on the power output is shown. In the literature, the selection of the stiffness of a linear harvester is generally referred to as frequency tuning of the harvester (Challa et al. 2008, Kim et al. 2000).

When specifying a harvester of known nonlinearity for a certain harmonic excitation source two parameters, namely linear stiffness and resistance, are relatively easy to adjust. A nonlinear harvester does not harvest maximum power when excited at its linear natural frequency — this occurs at the nonlinear resonant frequency. Nonetheless, it is possible to adjust the nonlinear resonant frequency by altering the underlying linear natural frequency. Here, using the same approach as for the previous discussion, the power output of the harvester is now maximized by selection of both the resistance and the linear stiffness.

This optimization can be used both to design a harvester of known nonlinearity once the characteristics of the external forces are known, or to develop a control strategy for devices which can be tuned to the external excitation.

4.1   Simplified formulas for two parameter-optimization

A possible solution for finding the maximum power when both the resistance and the stiffness of the system are variable is to extend the simplified method suggested in Section 3.4. By substituting Equation 24 into the expression for the power and then finding the extrema of the new function with respect to ω_n,

the following expression for the optimal value of ω_n is found

$$\omega_n^2 = \Omega^2 \left(1 - \frac{3}{16} \frac{m^2 Y_o^2 \alpha}{c_m^2} \right). \tag{29}$$

Note that this result is in agreement with the results found for the linear harvester. When $\alpha = 0$ the optimal ω_n is equal to the input frequency. When the stiffness is changed according to Equation (29) the power that the harvester provides is given by:

$$P_{opt} = \frac{1}{8} \frac{\Omega^4 Y_o^2 m^2}{c_m}. \tag{30}$$

This formula is the same as the maximum power obtainable from a linear harvester with variable stiffness Cammarano et al. 2010.

4.2 Numerical validation

The envelope of the maximum power provided by the simplified formula in Equation 30 has been validated using a numerical procedure based on continuation to solve Equation (8) directly. The procedure is identified by the following steps.

1. A frequency Ω_{opt} in the range [5-25] Hz is chosen as the frequency at which maximum power is required (take 20Hz as an example, dashed line in Figure 9a).

2. For a selected value of ω_n the power vs frequency response is evaluated (take ω_n= 10Hz, light grey in Figure 9a). Here,the resistance is chosen according to Equation (24) where $\Omega = \Omega_{opt}$.

3. The power harvested at optimum power is found and its value is stored for future comparison (grey bullet in the figure).

4. Further values of ω_n are selected and the maximum between the peak power and the maximum stored in the previous iteration is found by repeating steps 2 and 3.

5. The curve with the highest peak is the optimal response (black line in the figure) and the peak power is the maximum achievable power at Ω_{opt} (red dot in the figure).

6. Farther values of Ω_{opt} are considered and the envelope of the maximum power is found (red solid line in the figure) by repeating steps 1-5.

Note that in the linear case, Ω_{opt} and ω_n coincide as shown in Figure 9b. In the linear case the anlytical solution is exact. Figure 9c shows the comparison between the numerical and the analytical results. The error between the numerical and the analytical results is computed and shown in panel (d). Since the analytical results coincide with the optimal power of a linear harvester, panel (c) also provides a comparison between the linear and nonlinear harvester. As shown, if a nonlinear harvester can be tuned and the electrical load optimized, its power output is the same as that for an optimized linear harvester. Nevertheless, advantages of the nonlinear behavior stand. For example, the power

17

output of a nonlinear harvester drops more slowly than for the linear harvester because of the distorted peak. If the nonlinear harvester has a fixed optimized linear stiffness, its output would be the same as the linear one but the output is more robust to small deviations in the frequency content. In the case of a tunable nonlinear harvester, instead, this could be beneficial for the tuning system. In fact if the device is tuned only when the power drops below a fixed threshold, the nonlinear device needs to be tuned less frequently than the equivalent linear harvester. We note, however, the often cited drawback that with a nonlinear device there are multiple solutions for some frequencies and it must be ensured that the response remains on the upper branch.
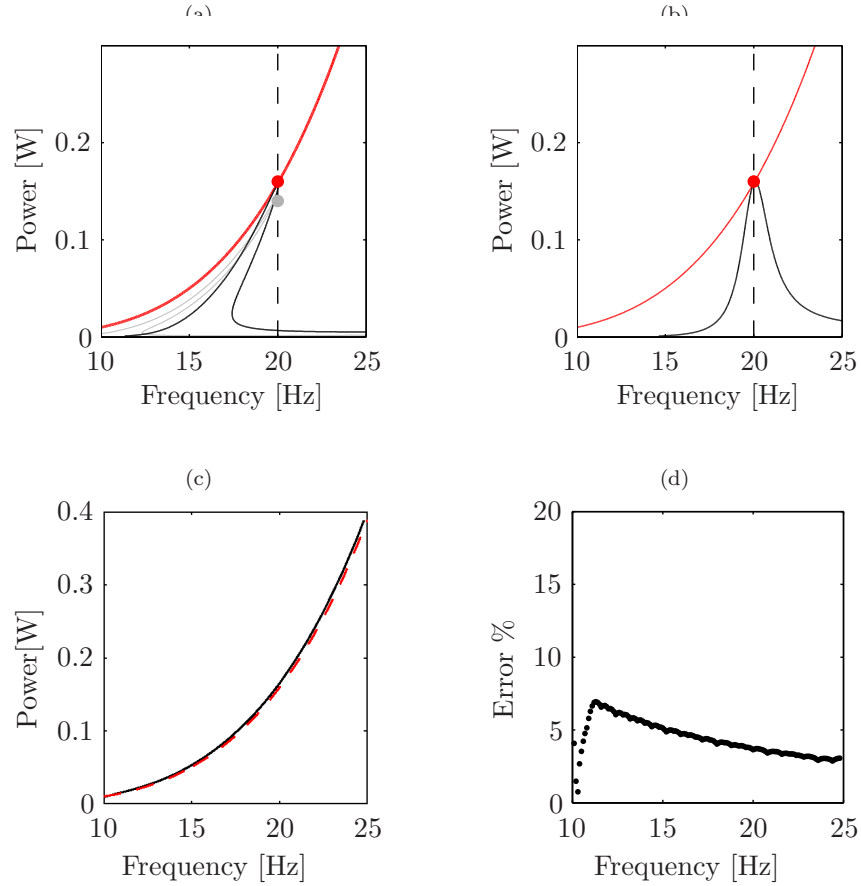

FIGURE 9: Two parameter optimization: Panel (a) and (b) show how the power versus frequency curves change as ω_n and R_L are optimized for different frequency of excitation in the nonlinear and linear case respectively. The envelope of the maxima of the power achieved changing both the resistive load and the stiffness of the harvester. The numerical results (solid black) and the results obtained with the simplified formula (dashed red) are superimposed (c). The percentage error introduced by the simplification is shown in (d).

18

5   Conclusion and future work

This work investigates the optimum load for energy harvesters. After a brief discussion on the optimum resistive load for a linear energy harvester, a method to extend the concept to nonlinear harvesters has been shown.

The study presents both an analytical and a numerical method. The analytical method utilizes the nonlinear normal forms technique and suggests a simplification based on the observation that the harvester delivers maximum power very close to the point at which the frequency response intersects the backbone curve, i.e. one of the fold points of the frequency response curve.

The optimum resistive load was computed and a comparison between the numerical and the analytical results was provided. The approximations made in the analytical method introduce a small error with the estimation of the power output and it provides a useful equation for estimating the resistive load for a nonlinear harvester.

Lastly a two-parameter optimization aimed at finding the stiffness and the resistive load that allow the harvester to generate maximum power was performed. The envelope of all the frequency-power curves was computed numerically and the result compared with the power values provided by a simplified formula based on the analytical method. The difference between the analytical and numerical result was never higher than 7%.

The simplified formula found with the analytical method is identical to that for an optimized linear harvester: the authors want to stress the importance of the implication of this result. Previous works have showed that the performance of a linear harvester at resonance is always better than that of a nonlinear harvester. However, for efficient performance over a range of input frequency, a linear harvester requires a tuning mechanism. Here we show that if a tuning mechanism is used on a nonlinear harvester, the power which can be harvested is almost identical. On the other hand, the advantage of a wider frequency bandwidth for nonlinear harvesters still stands, and this could be beneficial for the implementation of the tuning system.

Acknowledgments

References

Baker, J., Roundy, S. and Wright, P. 2005. Alternative geometries for increasing power density in vibration energy scavenging for wireless sensor networks, *3rd International Energy Conversion Engineering Conference. San Francisco, CA, USA*, pp. 1–12.

Barton, D. and Burrow, S. 2010. Numerical continuation in a physical experiment: Investigation of a nonlinear energy harvester, *Journal of Computational and Nonlinear Dynamics* **6**(1): 011010.

Burrow, S. and Clare, L. 2007. A resonant generator with non-linear compliance for energy harvesting in high vibrational environments, *Electric Machines & Drives Conference, 2007. IEMDC'07. IEEE International*, Vol. 1, IEEE, pp. 715–720.

Cammarano, A. 2012. *Increasing the bandwidth of resonant vibration-based energy harvesters*, PhD thesis, University of Bristol.

Cammarano, A., Burrow, S. and Barton, D. 2011. Modelling and experimental characterization of an energy harvester with bi-stable compliance characteristics, *Proceedings of the Institution of Mechanical Engineers, Part I: Journal of Systems and Control Engineering* **225**(4): 475–484.

Cammarano, A., Burrow, S., Barton, D., Carrella, A. and Clare, L. 2010. Tuning a resonant energy harvester using a generalized electrical load, *Smart Materials and Structures* **19**(5): 055003.

Challa, V., Prasad, M., Shi, Y. and Fisher, F. 2008. A vibration energy harvesting device with bidirectional resonance frequency tunability, *Smart Materials and Structures* **17**(1): 15035.

Cottone, F., Vocca, H. and Gammaitoni, L. 2009. Nonlinear energy harvesting, *Physical Review Letters* **102**(8): 080601.

Daqaq, M., Stabler, C., Qaroush, Y. and Seuaciuc-Osório, T. 2009. Investigation of power harvesting via parametric excitations, *Journal of Intelligent Material Systems and Structures* **20**(5): 545–557.

Doedel, E., Champneys, A., Fairgrieve, T., Kuznetsov, Y., Sandstede, B. and Wang, X. 1997. Auto 97: Continuation and bifurcation software for ordinary differential equations (with homcont).

Erturk, A., Hoffmann, J. and Inman, D. 2009. A piezomagnetoelastic structure for broadband vibration energy harvesting, *Applied Physics Letters* **94**(25): 254102.

Karami, M. and Inman, D. 2011. Equivalent damping and frequency change for linear and nonlinear hybrid vibrational energy harvesting systems, *Journal of Sound and Vibration* **330**(23): 5583–5597.

Kim, J., Ryu, Y. and Choi, S. 2000. New shunting parameter tuning method for piezoelectric damping based on measured electrical impedance, *Smart Materials and Structures* **9**(6): 868–877.

Liao, Y. and Sodano, H. 2009. Structural effects and energy conversion efficiency of power harvesting, *Journal of Intelligent Material Systems and Structures* **20**(5): 505–514.

Mann, B. and Sims, N. 2009. Energy harvesting from the nonlinear oscillations of magnetic levitation, *Journal of Sound and Vibration* **319**(1–2): 515–530.

20

Neild, S. and Wagg, D. 2011. Applying the method of normal forms to second-order nonlinear vibration problems, *Proceedings of the Royal Society A: Mathematical, Physical and Engineering Science* **467**(2128): 1141–1163.

Neild, S. and Wagg, D. 2013. A generalized frequency detuning method for multidegree-of-freedom oscillators with nonlinear stiffness, *Nonlinear Dynamics* **73**(1-2): 649–663.

Renno, J., Daqaq, M. and Inman, D. 2009. On the optimal energy harvesting from a vibration source, *Journal of Sound and Vibration* **320**(1): 386–405.

Roundy, S. and Wright, P. 2004. A piezoelectric vibration based generator for wireless electronics, *Smart Materials and Structures* **13**(5): 1131–1142.

Stanton, S., Erturk, A., Mann, B. and Inman, D. 2010. Nonlinear piezoelectricity in electroelastic energy harvesters: Modeling and experimental identification, *Journal of Applied Physics* **108**(7): 074903–074903.

Stephen, N. 2006. On energy harvesting from ambient vibration, *Journal of Sound and Vibration* **293**(1-2): 409–425.

Torah, R., Glynne-Jones, P., Tudor, M., O'Donnell, T., Roy, S. and Beeby, S. 2008. Self-powered autonomous wireless sensor node using vibration energy harvesting, *Measurement science and technology* **19**(12): 125202.

Triplett, A. and Quinn, D. 2009. The effect of non-linear piezoelectric coupling on vibration-based energy harvesting, *Journal of Intelligent Material Systems and Structures* **20**(16): 1959–1967.

Wickenheiser, A. and Garcia, E. 2010. Power optimization of vibration energy harvesters utilizing passive and active circuits, *Journal of Intelligent Material Systems and Structures* **21**(13): 1343–1361.

Williams, C. and Yates, R. 1996. Analysis of a micro-electric generator for microsystems, *Sensors & Actuators: A. Physical* **52**(1-3): 8–11.

Xin, Z., Neild, S., Wagg, D. and Zuo, Z. 2013. Resonant response functions for nonlinear oscillators with polynomial type nonlinearities, *Journal of Sound and Vibration* **332**(7): 1777 – 1788.